NIH Public Access
Author Manuscript
J Cell Physiol. Author manuscript; available in PMC 2014 August 11.

Published in final edited form as:
J Cell Physiol. 2013 July ; 228(7): 1594–1600. doi:10.1002/jcp.24322.

The Effects of GATA-1 and NF-E2 Deficiency on Bone Biomechanical, Biochemical, and Mineral Properties

Melissa A. Kacena[1,2,*], **Caren M. Gundberg**[2], **William J. Kacena III**[3], **William J. Landis**[4], **Adele L. Boskey**[5], **Mary L. Bouxsein**[6], and **Mark C. Horowitz**[2,**]

[1]Department of Orthopaedic Surgery, Indiana University School of Medicine, Indianapolis, Indiana

[2]Department of Orthopaedics and Rehabilitation, Yale University School of Medicine, New Haven, Connecticut

[3]Lockheed Martin, Littleton, Colorado

[4]Department of Polymer Science, University of Akron, Akron, Ohio

[5]Mineralized Tissues Laboratory, Hospital for Special Surgery, New York, New York

[6]Department of Orthopedic Surgery, Beth Israel Deaconess Medical Center, Boston, Massachusetts

Abstract

Mice deficient in GATA-1 or NF-E2, transcription factors required for normal megakaryocyte (MK) development, have increased numbers of MKs, reduced numbers of platelets, and a striking high bone mass phenotype. Here, we show the bone geometry, microarchitecture, biomechanical, biochemical, and mineral properties from these mutant mice. We found that the outer geometry of the mutant bones was similar to controls, but that both mutants had a striking increase in total bone area (up to a 35% increase) and trabecular bone area (up to a 19% increase). Interestingly, only the NF-E2 deficient mice had a significant increase in cortical bone area (21%) and cortical thickness (27%), which is consistent with the increase in bone mineral density (BMD) seen only in the NF-E2 deficient femurs. Both mutant femurs exhibited significant increases in several biomechanical properties including peak load (up to a 32% increase) and stiffness (up to a 13% increase). Importantly, the data also demonstrate differences between the two mutant mice. GATA-1 deficient femurs break in a ductile manner, whereas NF-E2 deficient femurs are brittle in nature. To better understand these differences, we examined the mineral properties of these bones. Although none of the parameters measured were different between the NF-E2 deficient and control mice, an increase in calcium (21%) and an increase in the mineral/matrix ratio (32%) was observed in GATA-1 deficient mice. These findings appear to contradict biomechanical findings, suggesting the need for further research into the mechanisms by which GATA-1 and NF-E2 deficiency alter the material properties of bone.

© 2013 Wiley Periodicals, Inc.

*Correspondence to: Melissa A. Kacena, Department of Orthopaedic Surgery, Indiana University School of Medicine, 1120 South Drive, FH 115, Indianapolis, IN 46202. mkacena@iupui.edu. **Correspondence to: Mark C. Horowitz, Department of Orthopaedics and Rehabilitation, Yale University School of Medicine, PO Box 208071, New Haven, CT 06520-8071. mark.horowitz@yale.edu.

Conflicts of interest: nothing to declare.

NIH-PA Author Manuscript
NIH-PA Author Manuscript
NIH-PA Author Manuscript

NIH-PA Author Manuscript

NIH-PA Author Manuscript

NIH-PA Author Manuscript

The molecular dissection of MK differentiation has been facilitated by the identification of transcription factors required for the cell to advance from stage to stage. Loss of these specific transcription factors arrests MK maturation at the latest stage of development prior to platelet formation. GATA-1 and NF-E2 are transcription factors which are restricted to cells in the hematopoietic lineage and are required for normal MK development. Mice deficient in either GATA-1 or NF-E2 develop a phenotype characterized by a marked increase in abnormal, immature MKs with a concomitant reduction in or absence of platelets (Shivdasani et al., 1995, 1997). Interestingly, these mice also develop a high bone mass phenotype with a greater than twofold increase in osteoblast (OB) number and trabecular bone volume (Kacena et al., 2004a, 2005). The similar phenotype, including the elevated numbers of OBs and MKs in both GATA-1 and NF-E2 deficient mice, led us to examine the potential interaction between OBs and MKs. In previous studies, we demonstrated that MKs stimulate OB proliferation (three- to six-fold) by a direct cell-to-cell contact mechanism (Kacena et al., 2004a; Ciovacco et al., 2009, 2010). These data suggest that the signaling mechanisms responsible for MK-induced anabolic bone formation may be a potential target for therapeutic treatment of bone loss diseases such as osteoporosis.

Because osteoporosis is a common age-related disease characterized by a decrease in bone mass and altered bone geometry, microarchitecture, and quality, it is important to examine not only bone volume in genetically altered mice, but also these other properties that influence bone fragility. Therefore, in the current study, we evaluated the geometry, microarchitecture, biomechanical properties, biochemical properties, and mineralization properties of bones from GATA-1 and NF-E2 deficient mice and their respective controls.

Materials and Methods

Mice

For these studies 5-month-old female mice were utilized. Generation and breeding of mutant mice with selective loss of NF-E2 or of MK-expressed GATA-1 were described previously (Shivdasani et al., 1995, 1997; McDevitt et al., 1997). In brief, a DNAse I-hypersensitive region (HS) was identified upstream of the GATA-1 promoter and was subsequently knocked-out by insertion of a neomycin-resistant cassette. This resulted in mice with reduced levels of GATA-1 mRNA and protein (three- to fivefold reduction in protein), a functional knock-down (McDevitt et al., 1997). GATA-1 deficient mice are maintained on the C57BL/6 background.

Generation and breeding of p45 NF-E2 deficient mice were described previously (Shivdasani et al., 1995). Briefly, to inactivate the p 45 NF-E2 gene, a PGK-neo cassette (NeoR) was inserted into the unique *Sal*l site upstream of the bZip encoding region (Shivdasani et al., 1995). The p45 NF-E2 deficient mice are maintained on the inbred 129/Sv genetic background.

All animal studies were performed with the approval of the Yale University IACUC and were conducted in accordance with the NIH guidelines.

NIH-PA Author Manuscript

NIH-PA Author Manuscript

NIH-PA Author Manuscript

μCT

Femurs were evaluated using a desktop micro-computerized tomographic (μCT) imaging system (μCT20, Scanco Medical AG, Brüttisellen; Ruegsegger et al., 1996). The entire femur was scanned using a 34-μm slice increment, requiring approximately 100–150 μCT slices per specimen. Images were reconstructed, filtered, and appropriate thresholds were applied (Alexander et al., 2001). Morphometric parameters were computed using a direct 3D approach that does not rely on any assumptions about the underlying bone structure (Hildebrand et al., 1999).

Microarchitecture analysis

Tibiae were fixed in 10% neutral-buffered formalin, dehydrated, and embedded in methylmethacrylate before being sectioned and stained with toluidine blue (Baron et al., 1984; Kacena et al., 2004b). Histomorphometric parameters (Parfitt et al., 1987) were analyzed by Osteomeasure software (Osteometrics, Decatur, GA).

Biomechanical testing

Three-point bending was used to assess biomechanical properties of the femur as previously described (Pearsall et al., 2008). Load was applied at a constant rate until failure (0.05 mm/sec). The peak load (N), bending stiffness (N/mm), and maximum stress (MPa) were determined.

Bone mineral density (BMD)

Whole body and femoral BMD (g/cm^2) was measured in vivo prior to sacrifice by peripheral DEXA (PIXImus, GE Lunar, Madison, WI).

Bone ashing

Tibiae were dissected and scraped free of muscle and soft tissue. Bones were washed in ice-cold water and the marrow flushed. Bones were lyophilized and then the bones of individual mice were pulverized by hand using a mortar and pestle. Dry weights were determined after heating at 100°C to constant weight. The bone powder was ashed in acid-washed crucibles at 600°C for 14h to constant weight. Bone ash (0.2–0.6 mg of bone powder) was dissolved in 0.5N HCl and the amount of calcium and inorganic phosphate was measured colorimetrically using a commercially available kit (Sigma, St. Louis, MO).

Fourier transform infrared imaging (FTIRI)

Tibiae were fixed in 90% ETOH and processed in methylmethacrylate (MMA) as previously described (Kacena et al., 2004b). Tibiae were sectioned on a Zeiss microtome at 2 μm thick and were examined by FTIRI using the Perkin Elmer Spotlight Imaging system (Perkin Elmer Instruments, Shelton, CT). The spectral resolution was either 4 or 16 cm^{-1}, and areas encompassing the region of the bone in question ($\sim 400 \times 400\ \mu m^2$) were examined. The spatial resolution was ~7 μm. Spectra were transferred to yield images corresponding to infrared band areas, peak height ratios, and integrated area ratios by a combination of instrument software and ISYS Chemical Imaging Software (v 2.1; Spectral Dimensions, Olney, MD, Marcott et al., 1998; Mendelsohn et al., 1999). Background spectra were

NIH-PA Author Manuscript

NIH-PA Author Manuscript

NIH-PA Author Manuscript

collected under identical conditions from the same BaF_2 windows. IR data of three areas per anatomical bone site at primary spongiosa, secondary spongiosa, and cortex were collected. After acquisition, spectra were truncated to allow analysis of the spectral data of interest and zero-corrected for the baseline, and the spectral contribution of PMMA embedding media was subtracted using ISYS software. Three spectroscopic parameters were calculated: mineral-to-matrix ratio, crystallinity, and collagen cross-link ratio (XLR). The mineral-to-matrix ratio (v1, v3 PO_4 band [900–1,200cm^{-1}]/amide I band [1,590–1,720cm^{-1}] integrated areas ratio) is a measure that corresponds to ash weight measurements (Boskey et al., 1992). Mineral crystallinity is a parameter that corresponds to the crystallite size and perfection as determined by X-ray diffraction, and it was calculated from the intensity ratios of subbands at 1,030 (stoichiometric apatite) and 1,020 cm^{-1} (nonstoichiometric apatite). XLR is a parameter reflecting the relative ratio of nonreducible and reducible collagen cross-links, expressed as the absorbance ratio at two specific wavenumbers (1,660 and 1,690 cm^{-1}; Paschalis et al., 2001). Details for the spectral processing methods and reproducibility of measurements are published elsewhere (Boskey et al., 1992; Marcott et al., 1998; Mendelsohn et al., 1999, 2000; Paschalis et al., 2001). In the spectral images, pixels devoid of bone (no mineral and/or matrix spectral signature) were set equal to zero and masked to be excluded from calculations. The spectroscopic results were expressed as histograms describing the pixel distribution of the three parameters above, mean values and standard deviations (SDs) of the pixel distribution, and corresponding color-coded images were generated at the same time by ISYS. Means and SDs were averaged for multiple sites in each animal and among five different animals for each age and genotype using Microsoft EXCEL.

X-ray crystallography

To identify the mineral crystal composition of GATA-1 deficient and counterpart control mouse bones, specimens were prepared for X-ray crystallographic analysis. The proximal and distal ends and midshafts of the femurs and tibiae from one GATA-1 deficient and one control mouse were dissected and separately lyophilized and ground to a powder with a mortar and pestle following the procedure described above for bone ashing. Bone powder obtained was packed into individual 1-mm diameter glass capillaries, which were then sealed and examined in a Brucker D-8 Advance powder Debye-Scherrer X-ray diffractometer with Cu Kα radiation. Scans were carried out for 24 h at 25°C in steps of 0.007° with a step time of 5 sec and 2θ range of 0–90°. Diffractograms were qualitatively examined and interpreted by comparison with Joint Committee on Powder Diffraction Standards (JCPDS) computerized files, including a representative inorganic hydroxyapatite. Width measurement at half maximum intensity of the 002 spectral reflection of apatite (20–26°) was utilized as a correlate of average crystal size of the respective powders (Prieto-Castello et al., 2007). An independent samples two-tailed *T*-test was used for statistical analysis of resulting data (IBM SPSS Statistics, version 20, Armonk, NY). Statistical significance was considered as $P \leq 0.05$.

Statistical testing

Unless otherwise noted, comparisons between control and mutant mice were made using analysis of variance (ANOVA). Post hoc comparisons between groups were accomplished

NIH-PA Author Manuscript

NIH-PA Author Manuscript

NIH-PA Author Manuscript

using a Fisher's protected least significant difference (PLSD) test or Student's *t*-test. Differences were considered significant at $P \leq 0.05$. Data are presented as mean ± SEM, unless indicated otherwise.

Results

Body weight and femur geometry

As summarized in Table 1, the average body weight for GATA-1 deficient mice was 25.4 ± 0.5 g, which was not significantly different from controls (25.4 ± 1.0 g). The average body weight for NF-E2 deficient mice was 24.0 ± 0.8 g, which was also not significantly different from their respective controls (23.6 ± 0.8 g).

With regard to femur geometry, there was no significant difference between mutant mice and their respective controls in terms of femur length (Table 1) or total cross-sectional area at the midshaft (Table 1 and Fig. 1A). However, as demonstrated in Figure 1B, there was a significant increase in bone area (BA, cortical bone + trabecular bone) in both mutant strains. The GATA-1 deficient mice had a 25.5% increase in BA ($P < 0.0001$) compared to controls, while the NF-E2 deficient mice realized a 34.8% increase in BA ($P < 0.0001$). With regard to trabecular bone area, GATA-1 deficient mice exhibited an 18.6% increase compared to controls ($P < 0.0001$) and NF-E2 deficient mice exhibited an 11.3% increase compared to controls ($P = 0.01$).

Interestingly, as shown in Figure 1C, although both mutant mice exhibited a striking increase in total bone area and trabecular bone area, cortical bone area was virtually identical between GATA-1 deficient mice and their controls, whereas in NF-E2 deficient mice, cortical bone area was significantly increased 20.7% ($P = 0.0002$). As demonstrated in Figure 1D, there was no significant difference in cortical thickness between GATA-1 deficient mice and controls; however, NF-E2 deficient mice displayed a 27.2% increase in cortical thickness compared to control mice ($P = 0.0001$).

Microarchitecture

With regard to microarchitecture, as summarized in Table 2, the trabecular bone volume was significantly increased 250% in GATA-1 ($P = 0.001$) and 127% in NF-E2 ($P = 0.001$) deficient mice compared to their respective controls. Trabecular number (Tb.N) was also significantly increased 206% in GATA-1 ($P = 0.002$) and 120% in NF-E2 ($P < 0.0001$) deficient mice. Because there was no difference in trabecular thickness (Tb.Th), as would be expected, trabecular spacing (Tb.Sp) was significantly reduced in both GATA-1 ($P = 0.03$) and NF-E2 ($P = 0.03$) deficient mice.

Femur biomechanical properties

As described above, the outer femur geometry was not different between mutant and control mice (length and total cross-sectional area). With a similar outer geometry but a striking increase in bone area, it would be predicted that the bones would be stronger and stiffer. This result was observed in both mutant mice (Fig. 2A,B). The GATA-1 deficient mice were 20.1% stronger than controls ($P = 0.002$) and the NF-E2 mice were 32.2% stronger ($P <$

NIH-PA Author Manuscript

NIH-PA Author Manuscript

NIH-PA Author Manuscript

0.0001) as determined by examining the peak load. Similarly, the GATA-1 deficient mice were 10.7% stiffer than controls ($P = 0.005$) and the NF-E2 deficient mice were 13.3% stiffer ($P = 0.001$). Even after correcting for geometry (maximum stress/ultimate strength), NF-E2 deficient femurs were still stronger and stiffer than controls, whereas GATA-1 deficient femurs were not (Fig. 2C).

The load versus deflection curve (Fig. 3) highlights another apparent difference between GATA-1 deficient and NF-E2 deficient bones. GATA-1 deficient femurs were more ductile, whereas NF-E2 deficient femurs were more brittle. Interestingly for NF-E2 deficient femurs, the load at yield, peak, and failure/break was essentially identical (∼34N), a result highlighting the brittle nature of these bones.

BMD

As illustrated in Figure 4, there was no detectable difference in whole body BMD when the mutant mice were compared to their respective controls. There was also no significant difference in the femoral BMD between GATA-1 deficient mice and controls. However, there was a significant 17.7% increase in BMD in the femur of NF-E2 deficient mice ($P = 0.006$). The increase seen with NF-E2 deficiency was consistent with the increase in cortical bone area and cortical thickness.

Biochemistry and mineral properties

Table 3 summarizes the biochemical properties (ashed calcium and phosphate ratios) and mineral properties (mineral/matrix, carbonate/matrix, crosslinks, and crystallinity) in mutant and control bones. For all the parameters examined there was no significant difference between NF-E2 deficient and control bones. However with GATA-1 deficiency, there was a significant 20.8% increase in calcium ($P < 0.0001$), resulting in a significant increase in the calcium/phosphate ratio. In addition, percent ash was increased 9.8% with GATA-1 deficiency ($P = 0.007$) compared to controls, whereas percent ash was similar between NF-E2 deficient and control bones. Consistent with the percent ash, the mineral/matrix ratio was also significantly elevated 32.4% in GATA-1 deficient mice ($P = 0.02$) but was similar between NF-E2 deficient and control mice.

As no differences in biochemical and mineral properties were observed between NF-E2 and control mouse bones, to understand further what was occurring in GATA-1 deficient bones we performed X-ray crystallography. Representative X-ray diffraction patterns of the mineral from lyophilized and powdered tibial midshafts of a GATA-1 deficient and control mouse are shown in Figure 5. The X-ray diffraction pattern from a synthetic inorganic hydroxyapatite of defined composition and high crystallinity is presented as a reference standard in each figure. Comparison of the individual patterns demonstrates that these two bone powders have diffraction reflections that correspond very closely to each other in their 2θ angle and to those of the synthetic hydroxyapatite. The bone powder diffraction peaks are also broader than those of the standard. These same diffraction characteristics are found for the mineral from the end regions and midshafts from all other tibiae and femurs of the GATA-1 deficient and control mice. On the basis of diffraction reflections, then, powders from the bone mineral of all mice are effectively indistinguishable. The synthetic

NIH-PA Author Manuscript

NIH-PA Author Manuscript

NIH-PA Author Manuscript

hydroxyapatite standard has direct 2θ correlation with the spectra from all powdered samples, a result indicating the bone mineral is also apatitic. Broadening of individual peaks of the powders defines the mineral as poorly crystalline compared to the highly crystalline nature of the standard.

Table 4 presents measurements of half maximum intensity peak widths of the apatite 002 reflections of individual bone powder specimens. Statistical analysis shows that the data are not significantly different ($P = 0.157$) when comparing all GATA-1 deficient bone samples with their counterpart controls (Table 4). In addition, there is no significant difference (data not shown) on comparing GATA-1 deficient and control femurs only ($P = 0.117$), GATA-1 deficient and control tibiae only ($P = 0.767$), all femurs and all tibiae ($P = 0.417$), GATA-1 deficient femurs and GATA-1 deficient tibiae ($P = 0.287$), control femurs and control tibiae ($P = 0.136$), GATA-1 deficient proximal and distal bone ends and control counterparts ($P = 0.337$), and GATA-1 deficient midshafts and control midshafts ($P = 0.281$).

Discussion

Because of the massive bone formation seen in GATA-1 and NF-E2 deficiency, it was important to characterize further the impact of these transcription factors on bone fragility. To this end we evaluated bone geometry and microarchitecture as well as biomechanical, biochemical, and mineralization properties for GATA-1 and NF-E2 deficient mice and their respective controls.

As detailed in Table 1 and Figure 1, the bone dimensions in mutant femurs are similar to those measured in controls. However, the total bone area and trabecular bone area are increased in both mutant femurs. An increase in bone area while the outer bone geometry remains unchanged would suggest that the bones would be stronger and stiffer. This precise result was found (Fig. 2). Although at first glance it appears that femurs from GATA-1 deficient mice are behaving in a manner similar to femurs from NF-E2 deficient mice, it becomes evident that distinct differences exist between these respective bones.

While the bone area is increased in both mutant femurs, only NF-E2 deficient femurs exhibit an increase in cortical bone area and cortical thickness. This difference explains why the femoral BMD is increased in NF-E2 deficiency but not in GATA-1 deficiency (Fig. 4). Importantly, whole body BMD is not elevated in either mutant, a result likely owing to the previously documented site-specific increase in bone volume (Kacena et al., 2005). Interestingly, even after correcting for differences in geometry, our data also suggest that NF-E2 deficient femurs are stronger and stiffer than control femurs (maximum stress/ ultimate strength). Such a result is likely attributable to the significant increase in cortical bone as it is well understood that the majority of the strength of a bone derives from its cortical component.

With regard to trabecular bone and microarchitecture, we find that, although both GATA-1 and NF-E2 deficient bones have a significant increase in trabecular bone, the increase is more pronounced with GATA-1 deficiency. As demonstrated in Table 2, the trabecular number is increased 206% with GATA-1 deficiency, whereas trabecular number is increased

NIH-PA Author Manuscript

NIH-PA Author Manuscript

NIH-PA Author Manuscript

120% with NF-E2 deficiency. It should be noted that these data were measured near the proximal end of the tibia. As we previously reported, the trabecular bone for the entire medullary canal (as assessed by μCT) was increased 150-fold with GATA-1 deficiency and 20-fold with NF-E2 deficiency (Kacena et al., 2004a). The striking increase in trabecular bone throughout the medullary canal is not usually observed and contributes to the increased strength of the bone.

Another striking difference between the biomechanical behavior of GATA-1 and NF-E2 deficient femurs is their energy absorbed to failure and their post-yield displacement. As depicted in Figure 3, these data suggest that NF-E2 femurs are more brittle and GATA-1 femurs are more ductile. Thus, we attempted to understand more completely the differences seen in post-yield energy and displacement. Because such differences can be explained by alterations in mineralization, we determined the calcium and phosphate ratios in ashed bones and we utilized FTIRI to examine the mineral properties of the bones.

As summarized in Table 3, no differences were observed between NF-E2 deficient and control mice in terms of calcium and phosphate ratios or FTIRI measurements. However, bones from GATA-1 deficient mice had higher levels of calcium and an increased mineral/matrix ratio. This finding is contrary to what we would expect given the biomechanical properties of the bones. We would predict that the brittle NF-E2 deficient bones would have a higher mineral/matrix ratio and/or altered mineral properties such as an altered calcium/phosphate ratio. We would also predict that the GATA-1 deficient bones would be undermineralized, a feature that would be consistent with the observed ductility. These seemingly contradictory findings suggest that further work is needed to explain the observed differences between NF-E2 and GATA-1 deficient mice in terms of their brittle and ductile behaviors. For example, it is possible that alterations in collagen may account for the observed differences.

In an attempt to clarify these findings further and because no differences in biochemical or mineral properties were observed between NF-E2 deficient and control mice, we then examined the X-ray diffraction patterns of GATA-1 deficient and control bones. As summarized in Table 4, X-ray diffraction patterns of the bone powders from the respective proximal and distal end portions or midshafts of femurs and tibiae from GATA and control animals were consistent with those of a poorly crystalline apatite. As a correlate of average crystal size, peak widths of the apatite 002 X-ray spectral reflection were not significantly different for all the bone mineral powders examined. Thus, although X-ray crystallography demonstrated that both C57BL/6 control and GATA-1 deficient mouse bones are poorly crystalline compared to a highly crystalline standard, the result that no distinguishable differences were detected in the identity of the bone mineral from these two representative specimens suggests that further work will be required to understand these observations.

Alternatively, it is possible that the variation in the background strain of the mice could contribute to the observed differences. It has been demonstrated that C3H/HEJ mice have a significant increase in both femoral BMD and femoral bone strength compared to C57BL/6J mice (Beamer et al., 1996; Turner et al., 2001). While the GATA-1 deficient mice are on a C57BL/6 genetic background, the NF-E2 deficient mice are on a 129/Sv genetic

NIH-PA Author Manuscript

NIH-PA Author Manuscript

NIH-PA Author Manuscript

background. It is possible that differences in the genetic background could be contributing to our observations. However, these possible factors need to be considered in relation to the observed increase in bone volume seen in both GATA-1 and NF-E2 deficiency.

In conclusion, we have demonstrated that GATA-1 and NF-E2 deficiency results in stronger and stiffer bones in the mice studied. In the case of GATA-1 deficiency, the increases appear to be a result of the increased trabecular bone present in the midshaft. For NF-E2 deficiency, it appears that the majority of the increase derives from the increase in cortical bone area and thickness. In addition to the difference in bone composition, the mutant mice differ in their inherent nature, whether they break in a brittle or ductile fashion. While we expected this difference to be explained directly by alterations in mineralization, we have instead found that a mineralization defect does not explain the biomechanical properties, a result suggesting that further research into the material properties of these bones must be conducted.

Acknowledgments

We would like to thank Drs. Stuart Orkin and Ramesh Shivdasani, both at the Dana-Farber Cancer Institute, for providing the GATA-1 and NF-E2 deficient mice, respectively. This work was supported in part by NIH/NIAMS grant R01 AR47342 (M.C.H.), R03 AR055269 (M.A.K.), R01 AR060332 (M.A.K.), P30 AR041621 (A.L.B.), R01 AR38460 (C.M.G.), and by a Pilot and Feasibility Award from the Yale Core Center for Musculoskeletal Disorders AR46032 (M.A.K.). The content in this manuscript is solely the responsibility of the authors and does not necessarily represent the official views of the NIH.

Contract grant sponsor: NIH/NIAMS;

Contract grant numbers: R01 AR47342, R03 AR055269, R01 AR060332, P30 AR041621, R01 AR38460, P30 AR46032.

Literature Cited

Alexander JM, Bab I, Fish S, Muller R, Uchiyama T, Gronowicz G, Nahounou M, Zhao Q, White DW, Chorev M, Gazit D, Rosenblatt M. Human parathyroid hormone 1–34 reverses bone loss in ovariectomized mice. J Bone Miner Res. 2001; 16:1665–1673. [PubMed: 11547836]

Baron R, Tross R, Vignery A. Evidence of sequential remodeling in rat trabecular bone: Morphology, dynamic histomorphometry, and changes during skeletal maturation. Anat Rec. 1984; 208:137–145. [PubMed: 6711834]

Beamer WG, Donahue LR, Rosen CJ, Baylink DJ. Genetic variability in adult bone density among inbred strains of mice. Bone. 1996; 18:397–403. [PubMed: 8739896]

Boskey AL, Pleshko N, Doty SB, Mendelsohn R. Applications of Fourier transform infrared (FT-IR) microscopy to the study of mineralization in bone and cartilage. Cell Mater. 1992; 2:209–220.

Ciovacco WA, Goldberg CG, Taylor AF, Lemieux JM, Horowitz MC, Donahue HJ, Kacena MA. The role of gap junctions in megakaryocyte-mediated osteoblast proliferation and differentiation. Bone. 2009; 44:80–86. [PubMed: 18848655]

Ciovacco WA, Cheng YH, Horowitz MC, Kacena MA. Immature and mature megakaryocytes enhance osteoblast proliferation and inhibit osteoclast formation. J Cell Biochem. 2010; 109:774–781. [PubMed: 20052670]

Hildebrand T, Laib A, Muller R, Dequeker J, Ruegsegger P. Direct three-dimensional morphometric analysis of human cancellous bone: Microstructural data from spine, femur, iliac crest, and calcaneus. J Bone Miner Res. 1999; 14:1167–1174. [PubMed: 10404017]

Kacena MA, Shivdasani RA, Wilson K, Xi Y, Troiano N, Nazarian A, Gundberg CM, Bouxsein ML, Lorenzo JA, Horowitz MC. Megakaryocyte-osteoblast interaction revealed in mice deficient in

NIH-PA Author Manuscript

NIH-PA Author Manuscript

NIH-PA Author Manuscript

transcription factors GATA-1 and NF-E2. J Bone Miner Res. 2004a; 19:652–660. [PubMed: 15005853]

Kacena MA, Troiano NW, Wilson KM, Coady CE, Horowitz MC. Evaluation of two different methylmethacrylate processing, infiltration, and embedding techniques on the histological, histochemical, and immunohistochemical analysis of murine bone specimens. J Histotech. 2004b; 27:119–130.

Kacena MA, Gundberg CM, Nelson T, Horowitz MC. Loss of the transcription factor p45 NF-E2 results in a developmental arrest of megakaryocyte differentiation and the onset of a high bone mass phenotype. Bone. 2005; 36:215–223. [PubMed: 15780947]

Marcott C, Reeder RC, Paschalis EP, Tatakis DN, Boskey AL, Mendelsohn R. Infrared microspectroscopic imaging of biomineralized tissues using a mercury-cadmium-telluride focal-plane array detector. Cell Mol Biol (Noisy-Le-Grand). 1998; 44:109–115. [PubMed: 9551643]

McDevitt MA, Shivdasani RA, Fujiwara Y, Yang H, Orkin SH. A “knockdown” mutation created by cis-element gene targeting reveals the dependence of erythroid cell maturation on the level of transcription factor GATA-1. Proc Natl Acad Sci USA. 1997; 94:6781–6785. [PubMed: 9192642]

Mendelsohn R, Paschalis EP, Boskey AL. Infrared spectroscopy, microscopy, and microscopic imaging of mineralizing tissues. Spectra-structure correlations from human iliac crest biopsies. J Biomed Opt. 1999; 4:14–21. [PubMed: 23015164]

Mendelsohn R, Paschalis EP, Sherman PJ, Boskey AL. IR microscopic imaging of pathological states and fracture healing of bone. Appl Spectrosc. 2000; 54:1183–1191.

Parfitt AM, Drezner MK, Glorieux FH, Kanis JA, Malluche H, Meunier PJ, Ott SM, Recker RR. Bone histomorphometry: Standardization of nomenclature, symbols, and units. Report of the ASBMR Histomorphometry Nomenclature Committee. J Bone Miner Res. 1987; 2:595–610. [PubMed: 3455637]

Paschalis EP, Verdelis K, Doty SB, Boskey AL, Mendelsohn R, Yamauchi M. Spectroscopic characterization of collagen cross-links in bone. J Bone Miner Res. 2001; 16:1821–1828. [PubMed: 11585346]

Pearsall RS, Canalis E, Cornwall-Brady M, Underwood KW, Haigis B, Ucran J, Kumar R, Pobre E, Grinberg A, Werner ED, Glatt V, Stadmeyer L, Smith D, Seehra J, Bouxsein ML. A soluble activin type IIA receptor induces bone formation and improves skeletal integrity. Proc Natl Acad Sci USA. 2008; 105:7082–7087. [PubMed: 18460605]

Prieto-Castello MJ, Hernandez del Rincon JP, Perez-Sirvent C, Alvarez-Jimenez P, Perez-Carceles MD, Osuna E, Luna A. Application of biochemical and X-ray diffraction analyses to establish the postmortem interval. Forensic Sci Int. 2007; 172:112–118. [PubMed: 17306944]

Ruegsegger P, Koller B, Muller R. A microtomographic system for the nondestructive evaluation of bone architecture. Calcif Tissue Int. 1996; 58:24–29. [PubMed: 8825235]

Shivdasani RA, Rosenblatt MF, Zucker-Franklin D, Jackson CW, Hunt P, Saris CJ, Orkin SH. Transcription factor NF-E2 is required for platelet formation independent of the actions of thrombopoietin/MGDF in megakaryocyte development. Cell. 1995; 81:695–704. [PubMed: 7774011]

Shivdasani RA, Fujiwara Y, McDevitt MA, Orkin SH. A lineage-selective knockout establishes the critical role of transcription factor GATA-1 in megakaryocyte growth and platelet development. EMBO J. 1997; 16:3965–3973. [PubMed: 9233806]

Turner CH, Hsieh YF, Muller R, Bouxsein ML, Rosen CJ, McCrann ME, Donahue LR, Beamer WG. Variation in bone biomechanical properties, microstructure, and density in BXH recombinant inbred mice. J Bone Miner Res. 2001; 16:206–213. [PubMed: 11204420]

NIH-PA Author Manuscript
NIH-PA Author Manuscript
NIH-PA Author Manuscript

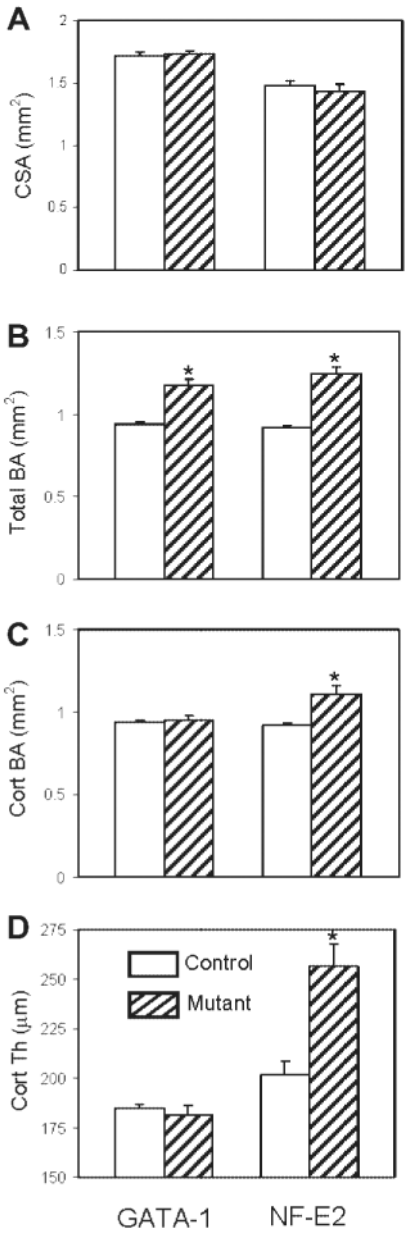

Fig. 1.

Femoral geometry measured in GATA-1 deficient, NF-E2 deficient, and control mice. Mean values for midfemoral (A) total cross-sectional area inside the periosteal envelope (CSA, mm^2), (B) cortical and trabecular bone area within this same envelope (BA, mm^2), (C) cortical bone area (Cort BA, mm^2), and (D) cortical thickness (Cort Th, μm) were assessed by μCT. Open boxes represent control bones and cross-hatched boxes represent mutant bones (GATA-1 or NF-E2 deficient). Error bars represent the SEM (n = 9–15). *Significant difference from respective control, $P < 0.05$.

NIH-PA Author Manuscript
NIH-PA Author Manuscript
NIH-PA Author Manuscript

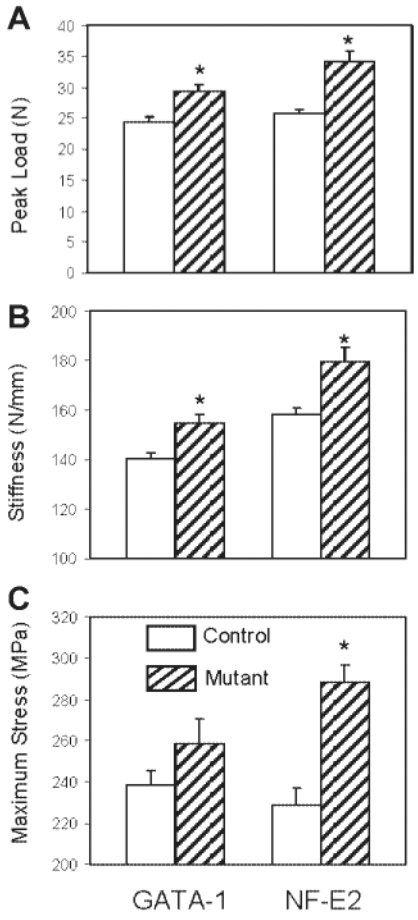

Fig. 2.

Femoral biomechanical properties for GATA-1 deficient, NF-E2 deficient, and control mice. Mean values for midfemoral (A) peak load (N), (B) stiffness (N/mm), and (C) maximum stress (MPa) were assessed by 3-point bending analysis. Open boxes represent control bones and cross-hatched boxes represent mutant bones. Error bars represent the SEM (n = 9–15). *Significant difference from respective control, $P < 0.05$.

NIH-PA Author Manuscript
NIH-PA Author Manuscript
NIH-PA Author Manuscript

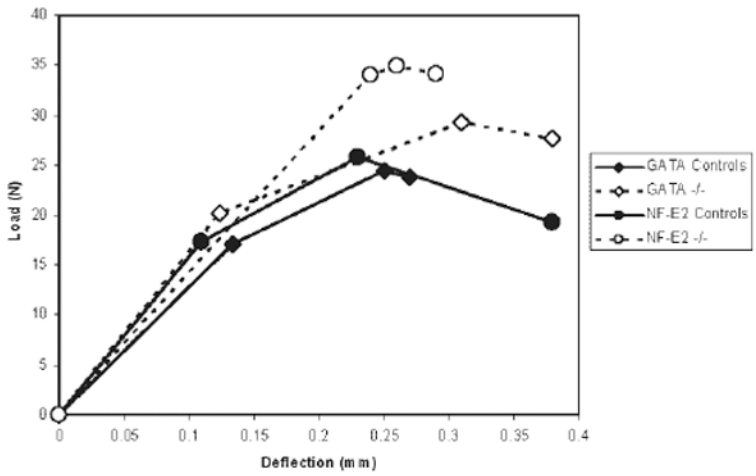

Fig. 3.

Load versus deflection curve for GATA-1 deficient, NF-E2 deficient, and control mice. The first point is at yield, the second point is at peak, and the final point is at failure.

NIH-PA Author Manuscript

NIH-PA Author Manuscript

NIH-PA Author Manuscript

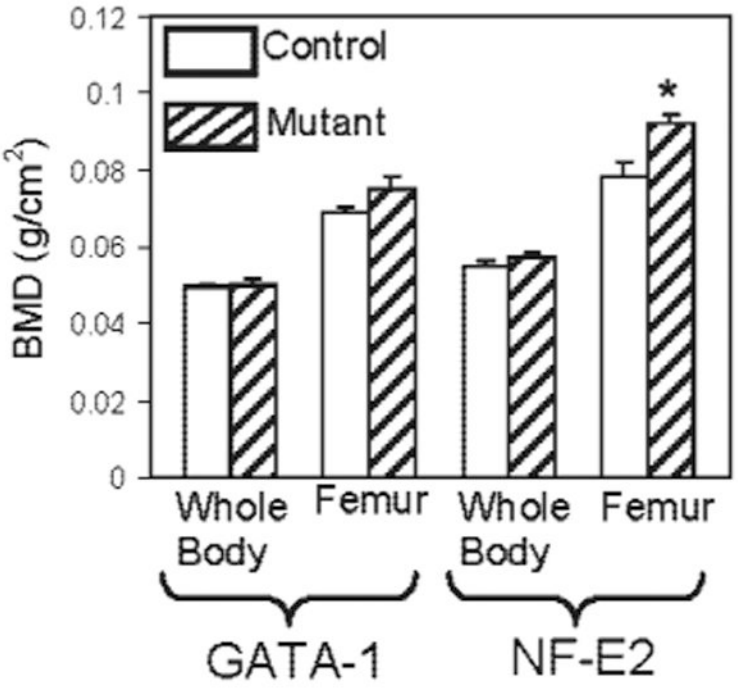

Fig. 4.

Mean whole body and femoral BMD in GATA-1 deficient, NF-E2 deficient, and control mice were assessed by peripheral DEXA. Open boxes represent control bones and cross-hatched boxes represent mutant bones. Error bars represent the SEM (n = 9–15).

*Significant difference from respective control, $P < 0.05$.

NIH-PA Author Manuscript
NIH-PA Author Manuscript
NIH-PA Author Manuscript

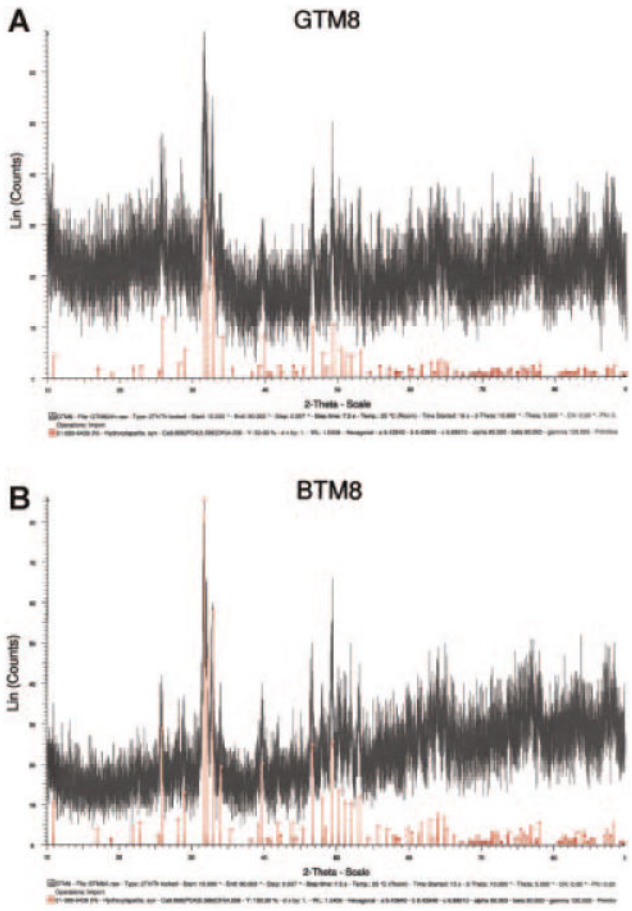

Fig. 5.

Representative X-ray diffractograms of GATA-1 deficient (A) and control (B) mouse bone powder (black trace) compared to a synthetic inorganic hydroxyapatite of known composition (red trace). Diffraction reflections from the powders correspond to that of a poorly crystalline apatite (reflections are broader than those of the synthetic hydroxyapatite).

NIH-PA Author Manuscript

NIH-PA Author Manuscript

NIH-PA Author Manuscript

Table 1

Body weight and femur geometry for GATA-1 deficient, NF-E2 deficient, and control mice

Type	n	Body weight (g)	Femur length (mm)	Total cross-sectional area
GATA-1 controls	9	25.4±1.0	15.8±0.5	1.71±0.03
GATA-1 −/−	13	25.4±0.5	15.5±0.7	1.73±0.03
NF-E2 controls	15	23.6±0.8	16.3±0.6	1.48±0.03
NF-E2 −/−	9	24.0±0.8	16.1±0.3	1.43±0.06

Data are presented as mean ± SEM.

* No significant differences were detected.

NIH-PA Author Manuscript
NIH-PA Author Manuscript
NIH-PA Author Manuscript

Table 2

Microarchitecture of bones for GATA-1 deficient, NF-E2 deficient, and control mice

Type	n	BV/TV (%)	Tb.N (mm^{-1})	Tb.Th (μm)	Tb.S (μm)
GATA-1 controls	9	4±1	1.6±1.4	24±2	808±318
GATA-1 −/−	6	14±3*	4.9±1.1*	32±5	182±53*
NF-E2 controls	5	15±5	5±1	30±4	197±71
NF-E2 −/−	4	34±2*	11±1	31±2	61±4*

Data presented as mean ± SD.

*Significant difference from respective controls, $P < 0.05$.

J Cell Physiol. Author manuscript; available in PMC 2014 August 11.

NIH-PA Author Manuscript
NIH-PA Author Manuscript
NIH-PA Author Manuscript

Table 3

Biochemical and mineral properties of bones for GATA-1 deficient, NF-E2 deficient, and control mice

Type	n	mg Ca/mg BP	mg P/mg BP	Mineral/Matrix	Carbonate/Matrix	Crosslinks	Crystallinity
GATA-1 controls	5–6	0.24±0.02	0.14±0.01	7.1±0.7	0.009±0.001	3.3±0.3	1.11±0.07
GATA-1 −/−	4–6	0.29±0.04*	0.15±0.02	9.4±1.4*	0.009±0.001	3.8±0.4	1.16±0.03
NF-E2 controls	5–6	0.28±0.01	0.18±0.01	7.9±1.4	0.0076±0.0003	3.2±0.4	1.14±0.04
NF-E2 −/−	4–6	0.28±0.02	0.18±0.01	8.3±1.2	0.0084±0.0000	3.4±0.6	1.17±0.09

Data presented as mean ± SD.

*Significant difference from respective controls, $P < 0.05$.

NIH-PA Author Manuscript
NIH-PA Author Manuscript
NIH-PA Author Manuscript

Table 4
Peak width measurements for GATA-1 deficient and control bone powders

Specimen	Width at 002 half maximum intensity (degrees 2θ)
BFE8	0.443
BFE9	0.423
BFM8	0.616
BFM9	0.440
BTE8	0.371
BTE9	0.393
BTM8	0.417
BTM9	0.419
GFE7	0.420
GFE8	0.291
GFM7	0.398
GFM8	0.414
GTE7	0.374
GTE8	0.407
GTM7	0.492
GTM8	0.392

Key to specimens: Control mice (B), GATA-1 deficient mice (G), femur (F), tibia (T), proximal and distal end portions of bone (E), midshaft of bone (M). Numbers 7–9 identify individual mice.